

Free-Floating Planets and Binaries in Stellar Clusters

FANGYUAN YU  ^{1,2} AND DONG LAI  ^{3,4}

¹ *Zhiyuan College, Shanghai Jiao Tong University, 800 Dongchuan Road, Minhang, Shanghai 200240, China*

² *School of Physics and Astronomy, Shanghai Jiao Tong University, 800 Dongchuan Road, Minhang, Shanghai 200240, China*

³ *Center for Astrophysics and Planetary Science, Department of Astronomy, Cornell University, Ithaca, NY 14853, USA*

⁴ *Tsung-Dao Lee Institute, Shanghai Jiao-Tong University, Shanghai, 520 Shengrong Road, 201210, China*

ABSTRACT

TBD...

Keywords: Exoplanet dynamics(490)

1. INTRODUCTION

In the near-infrared survey of the inner Orion Nebula and Trapezium Cluster conducted by the James Webb Space Telescope (Pearson & McCaughrean 2023), researchers discovered that a surprising 9% of planetary mass objects exist in wide binaries. This finding contradicts current theories of star and planet formation, adding a challenging element to our understanding of these processes.

Recent work (Wang et al. 2024) suggested that bound binaries could be produced by stellar flyby, and calculated ratio of the cross section of JuMBOs production to that of single ejected free-floating planets can approach 20% on certain conditions. However, they didn't give a clear indication of how likely this is to happen in the entire cluster. In this article, we will analyze this issue. We have a star orbiting two planets in our system, and a stellar flyby passing by at the same time. In the analysis of this circumstance, we are concerned about three main questions: (1) what is the velocity distribution of single free-floating planet; (2) what is the probability of forming Jupiter Mass Binary Objects (JuMBOs); (3) what are the orbital parameters of the gravitational binding system after the flyby perturbation.

2. METHOD

Studying the chaotic effects of a flyby with a smaller periastron requires numerical analysis. Therefore, we utilize N-body simulations employing the IAS15 integrator from the REBOUND package (Rein & Liu 2012); (Rein & Spiegel 2015) for this purpose.

2.1. *Simulation setup*

To limit the number of parameters, the simulations include two equal-mass stars $M_1 = M_2 = M_{\odot}$ and two equal-mass Jupiters $m_1 = m_2 = M_J$. Our simulation encompasses a period ranging from $50 t_0$ of time before (about $30 a_2$ away) the flyby periastron to $500 t_0$ after (about $500 a_2$ away). $t_0 = \sqrt{\frac{a_2^3}{GM_1}}$, where a_2, a_1 represents the semi-major axis of the outer planet and inner planet respectively. The simulation time-step is adaptive.

For stars M_1 and M_2 approaching each other with relative velocity v_{∞} , the velocity at periastron q is given by

$$\begin{aligned} v_{\text{peri}}^2 &= v_{\infty}^2 + \frac{2GM_{\text{tot}}}{q} \\ &= v_{\infty}^2 + (10 \text{ km s}^{-1})^2 \left(\frac{50 \text{ au}}{q} \right) \left(\frac{M_{\text{tot}}}{2M_{\odot}} \right) \end{aligned} \quad (1)$$

where $M_{\text{tot}} = M_1 + M_2$. In our simulations, we utilize an eccentricity value of 1.1 for all encounters. We have verified that the effects of the flybys exhibit little variation with e , as long as it stays in proximity to 1. For the distance between planets, we choose $\alpha = \frac{a_1}{a_2} = 0.7$, as 0.7 satisfies the conditions for orbital stability in Equation (2).

$$a_2 - a_1 > 2\sqrt{3} R_{\text{Hill}} = 2\sqrt{3} \frac{a_1 + a_2}{2} \left(\frac{m_1 + m_2}{3M} \right)^{\frac{1}{3}} \quad (2)$$

36 In addition to the periastron distance $q = \frac{a_p}{a_2}$, the outcome of a flyby depends on the inclination i between the flyby
 37 orbital plane and the initial orbital plane of the companion, ω , the argument of periastron, λ_{p1} , the initial orbital
 38 phase of the outer planet, and λ_{p2} , the initial orbital phase of the inner planet. Note that since the initial companion
 39 orbit is circular, the outcome of an encounter does not depend on Ω , the longitude of the node. In our simulations,
 40 we sample the periastron q over a uniform grid from 0.1 to 2 except a detailed survey of $q < 0.1$, and choose

- 41 1. i , with a $\sin(i)$ probability distribution, between 0 and π ,
 42 2. ω , with a flat prior between 0 and 2π ,
 43 3. λ_{p1} , with a flat prior between 0 and 2π .
 44 4. λ_{p2} , with a flat prior between 0 and 2π

45 For each value of q , we sample $20 \times 20 \times 20 \times 20$ angles (for i , ω , λ_{p1} , and λ_{p2}) to determine the distributions of
 46 post-flyby orbital parameters of the companion.

47 2.2. Branching criteria

48 Both planets could each be kicked out of their original star system, or they could remain in their original system.
 49 The kicked planet could become a free-floating planet, or it could be captured by the flyby, which we call the Stolen
 50 Planet. If both planets are kicked out at the same time, it is also possible to form a free-floating binary, also known
 51 as JuMBO, which is of particular interest to us.

52 It is necessary for us to evaluate how we differentiate between a planet being a free-floating planet, a stolen planet,
 53 or a free-floating binary. Our branching criteria are:

- 54 • Free-floating: the separation between the planet and both stars exceeds $50 a_1$, and the total energy relative to
 55 both stars is positive.
- 56 • Exchange: the separation between the planet and the initial star exceeds $50 a_1$, while the separation between the
 57 planet and the flyby is less than $50 a_1$. Its energy is positive relative to the original star and negative relative to
 58 the flyby.
- 59 • Free-floating binary: the separation between the planets is less than half Hill radius $r_{\text{Hill}} = (\frac{2m}{3M})^{\frac{1}{3}} d$, where d
 60 is the minimum separation between every planet and star, this indicates that the gravitation between planets
 61 dominates their motion. The relative energy between the two planets is negative, and the separation between
 62 both planet and both star exceeds $50 a_1$.
- 63 • Remain bound: the separation between the planet and the initial star is less than $50 a_1$, and its energy is negative
 64 relative to the original star.

65 We will categorize the outcomes $400 t_0$ after the periastron and double-check at $500 t_0$. Only results that match will
 66 be recorded, while any discrepancies will be noted as anomalies. The parameters in our criteria have been optimized
 67 to the extent that the probability of anomalies is negligible and can be disregarded.

68 3. NUMERICAL RESULT

69 In this section, we will introduce the results of the simulation as well as the data analysis. In 3.1 we will analyze the
 70 likelihood of various scenarios occurring; In 3.2 we will analyze the velocity distribution of the resulting free-floating
 71 planet. In 3.3 we will analyze the single planet created after a perturbation when a planet in the protoplanetary system
 72 is kicked out. In 3.4 we will analyze the orbital parameter distribution of the double planet when it is still a double
 73 planetary system after perturbation. In 3.5 we will analyze the orbital parameter distribution of the planet captured
 74 by flyby (stolen planet) relative to flyby. In 3.6 we will analyze the orbital parameter distribution of flyby induced
 75 JuMBO.

76 3.1. Branching ratio

77 By simulating q 's uniform grid from 0.1 to 2, we get different probabilities of the result. For the very small q ($q < 0.1$),
 78 we simulated 0.002 – 0.005 separately (with a sun radius of 4.67×10^{-5}) and got clearer results. At the same time,
 79 we analyzed both the inner planet and the outer planet, and obtained Figure 1(a) and Figure 1(b). It is generally
 80 assumed that the gravitational forces between planets within this system are significantly smaller than those between
 81 the planets and the stars. We can define $\tilde{q} = \frac{a_p}{a_i}$, rescale the results of the inner planet and compare the results of this
 82 rescaled with the results of the outer planet to test this hypothesis.

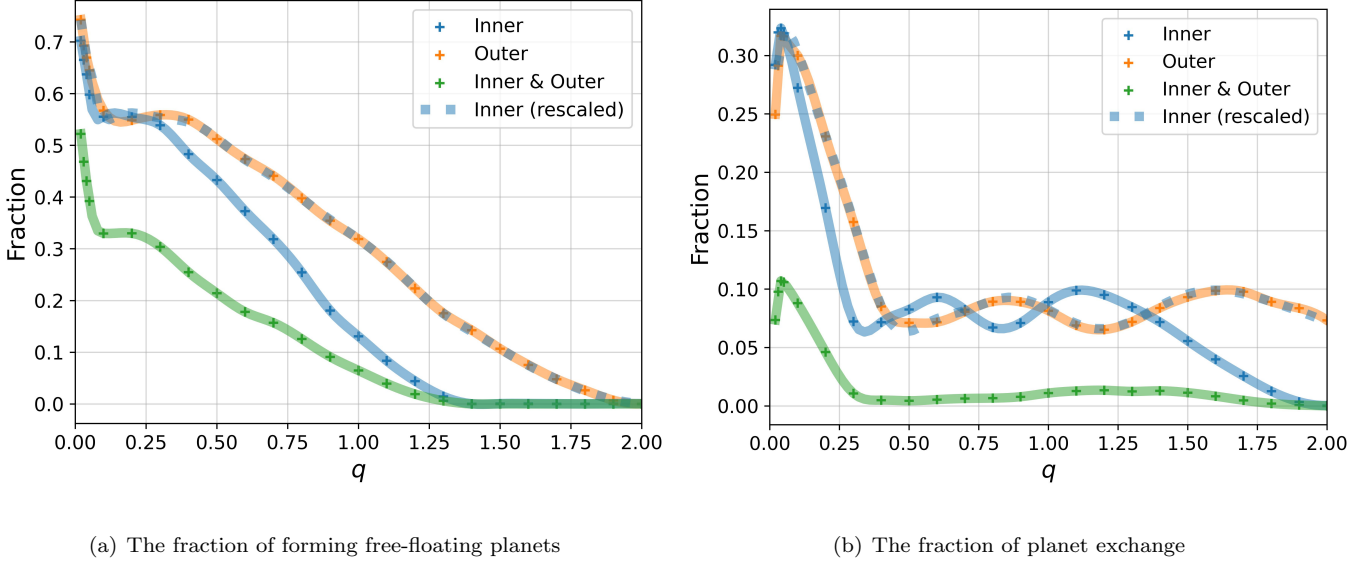


Figure 1. The solid blue line in the figure is the fraction of the inner planet being kicked out to form the free-floating planet or a planet exchange; The orange line is the fraction of the outer planet being kicked out. The green line is the fraction where both planets are kicked out and become free-floating planets or both be captured by the flyby. The blue dotted line is the curve of the inner planet after rescale, with \tilde{q} as the abscissa, which is in good agreement with the curve of the outer planet in both figure. This result indicates that our hypothesis is valid.

83 When q is small ($0.1 < q < 0.3$), we observe that the fraction of forming a free-floating planet suddenly ceases to
 84 increase as q decreases. Instead, the fraction of planet exchange experiences a sudden increase. In fact, if we add
 85 up the fractions of the two, i.e., consider all the fractions of planets becoming unbound, it continues to increase as q
 86 decreases. (Regarding the increase in the fraction of planet exchange, it may be due to the flyby staying longer in the
 87 planet's orbit when it is very close to the original star, thereby having a greater fraction of capturing the planet.)

88 Furthermore, at $\alpha = 0.7$, there is an exceedingly small probability of forming a free-floating binary. Due to the very
 89 low probabilities, the number formed in the simulation is also very small, leading to significant fluctuations in the
 90 data. To address this, we sampled $30 \times 30 \times 30 \times 30$ angles (for i , ω , λ_{p1} , and λ_{p2}) to obtain additional examples. The
 91 results of both simulations are plotted in Figure 2 to provide a rough idea of the impact of data fluctuations.

93 3.2. Property of free-floating planet

94 For free-floating planets, what we are interested in are velocities within the center-of-mass frame of the stellar cluster.
 95 Ideally, if we neglect the influence of planetary momentum and consider that the flyby's velocity at infinity should be
 96 close to 0, the simulation reference frame is essentially the center-of-mass frame. However, since we start the simulation
 97 at a distance of around 30 a.u., there exists a certain relative velocity between our simulation reference frame and the
 98 center-of-mass frame. Consequently, we can compute the velocities of free-floating planets relative to the center of
 99 mass of the star and the flyby at the end of the simulation. This is a good approximation for the velocities in the
 100 center-of-mass frame of the stellar cluster. Under such conditions, v_∞ can be expressed as Equation (3):

$$v_\infty = \sqrt{\left| \vec{v}_{\text{end}} - \frac{\vec{V}_1 + \vec{V}_2}{2} \right|^2 - \frac{2GM_1}{r_1} - \frac{2GM_2}{r_2}} \quad (3)$$

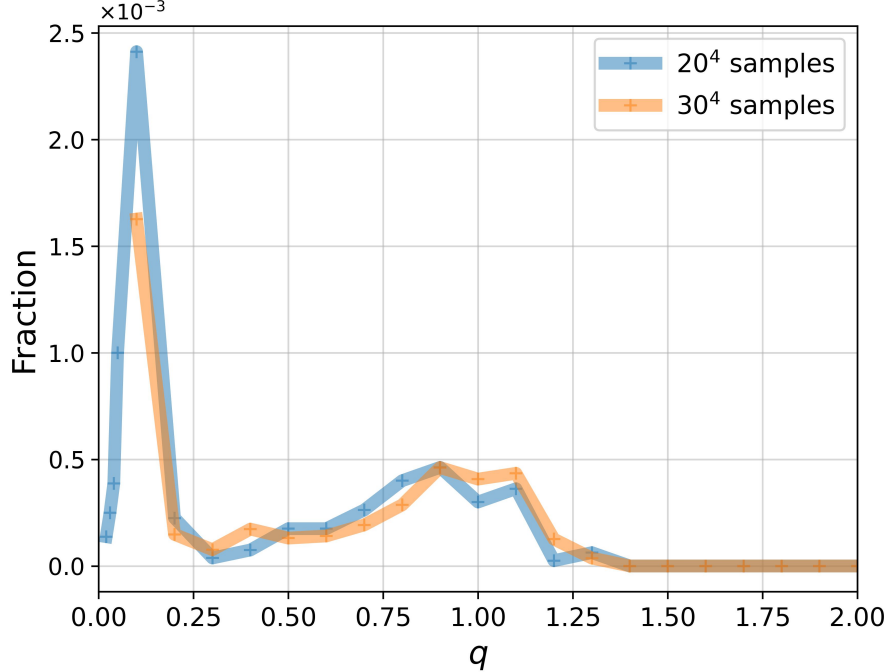


Figure 2. The fraction of forming Jupiter Mass Binary Objects (JuMBOs). As can be seen from the figure, there is a sharp peak in the probability of JuMBO formation at $q = 0.1$, and the probability will reach about 0.2%. Then the fraction decreases greatly with the increase of q , but another diffuse peak appears around $q = 1.0$, and the probability of JuMBO formation is about 0.04%. JuMBO will no longer be formed when $q > 1.5$. Data perturbations do not significantly affect our conclusions.

where \vec{v}_{end} , \vec{V}_1 , and \vec{V}_2 represent the velocities of the free-floating planet, original star, and flyby relative to the simulation reference frame at the end of the simulation, respectively. Obviously, $\frac{\vec{V}_1 + \vec{V}_2}{2}$ is the velocity of the center-of-mass relative to the simulation reference frame.

We analyzed all the generated free-floating planets in the simulation and obtained probability density functions (PDFs) for the velocity distributions of free-floating planets produced with different initial semi-major axis in Figure 3. We can roughly think of $v_{\infty} \sim \sqrt{\frac{GM}{a_i}}$, so we rescale v_{∞} using the unit of $\sqrt{\frac{GM}{a_i}}$. The results reveal that planets from different orbits exhibit consistency in velocity distribution after becoming free-floating planets, aligning with the semi-major axis of their original orbits.

3.3. Property of single surviving planet

After a significant gravitational disturbance, one of the many planets in the dual planet planetary system will be kicked out of the original system and become a free-floating planet, or be captured by the flyby. This will result in some single planet systems, and we hope to analyze these systems. We first analyzed the planet according to whether it was an inner planet or an outer planet in the first place. Then, considering that we cannot know whether a single planetary system is inner one or outer one if it is formed by a flyby at the time of actual observation, we will consider the orbital parameters of all single-planetary systems that have been formed, regardless of whether it was originally inner planet or outer planet.

Firstly, we plot the semi-major axis and the eccentricity of inner and outer only survivors respectively in Figure 4.

We expect to see a large dispersion on the semi-major axis after the perturbation, but the peak should be consistent with the initial value. This will result in a clear distinction between inner survivors and outer survivors, but we should be able to solve this problem with rescaling method mentioned before. However, from Figure 4(a) we can see that there is no clear distinction between inner survivors and outer survivors. This indicates that the peak value of the semi-major axis has a certain inward migration when the disturbance is large. This is consistent with the results of Figure 3 in (Rodet et al. 2021). For eccentricity, we would expect the inner and outer survivors to be similar, but we also see different behaviors from Figure 4(b). The reason for this trend is that the distribution of eccentricity is very different for different q . As q changes from large to small, the peak of eccentricity will slowly increase from 0 to 1, and

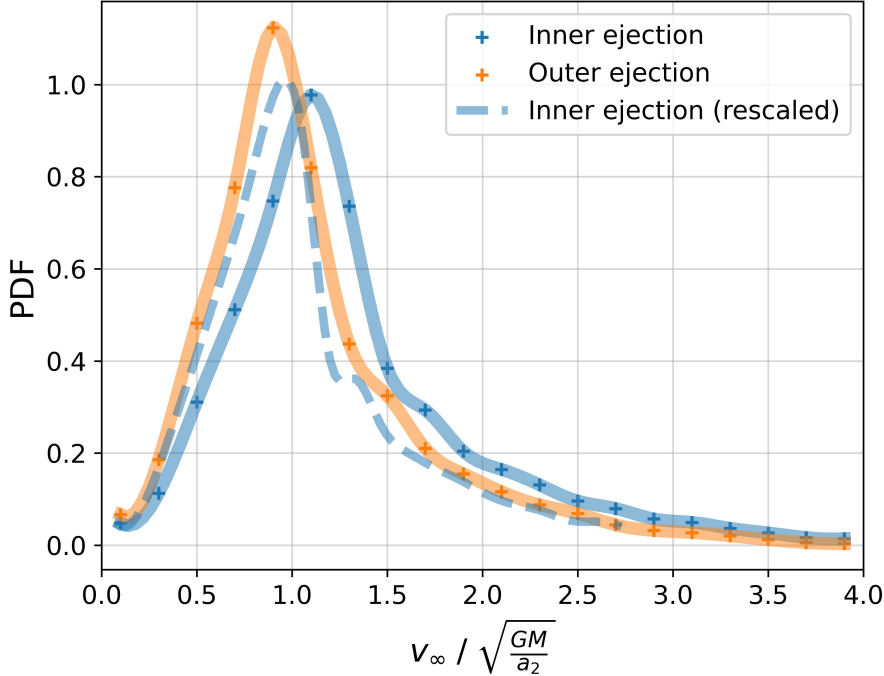


Figure 3. v_∞ distribution for free-floating planets. The blue dashed line is the velocity distribution of the free-floating planet formed by the inner planet ejection after rescaling. It matches the solid orange line, which is the velocity distribution of the free-floating planet formed by the outer planet ejection.

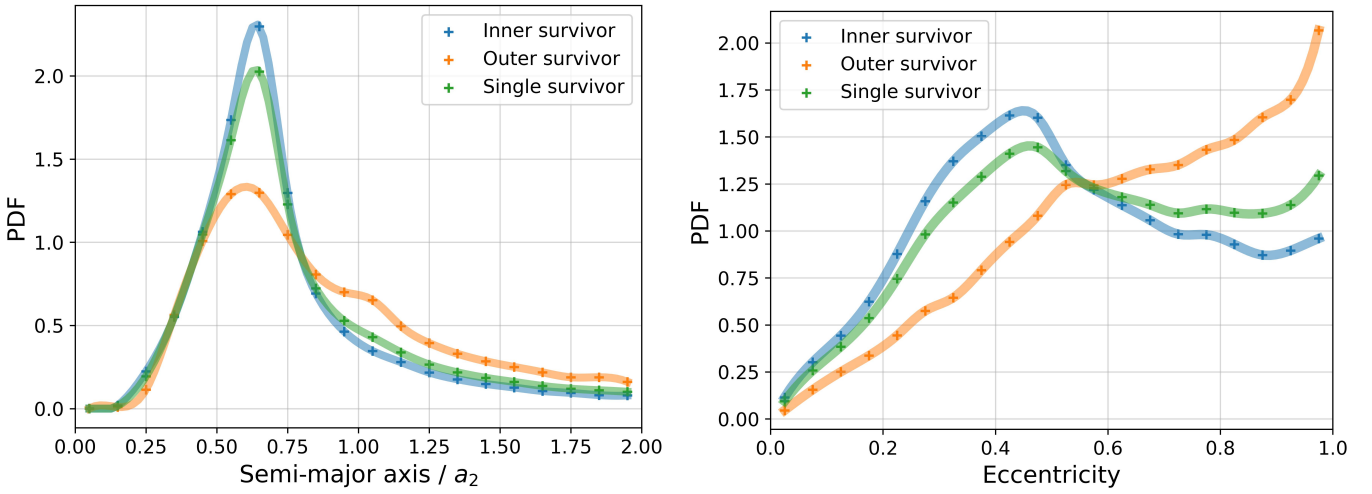


Figure 4. Single planet system orbital parameter distribution. Blue and orange line indicate that the planet in the single planet system starts out as the inner planet or the outer planet. Green line is an analysis of all orbital parameters of the single planet system, regardless of the initial situation.

the dispersion of the distribution will gradually increase. The detailed analysis of this part is discussed in B, which is also consistent with the results of Figure 3 in (Rodet et al. 2021).

We can also get the $e - a$ plot for the single planet system in Figure 5. Here and later in the $e - a$ plot we can see some similar common features, such as the fact that it seems that all the orbital parameters are in a zone. The outside of the zone, which is the white part of the diagram, is a forbidden zone. There is an envelope between this, and is it possible to write the equation? $a(1 + e) = constant$?

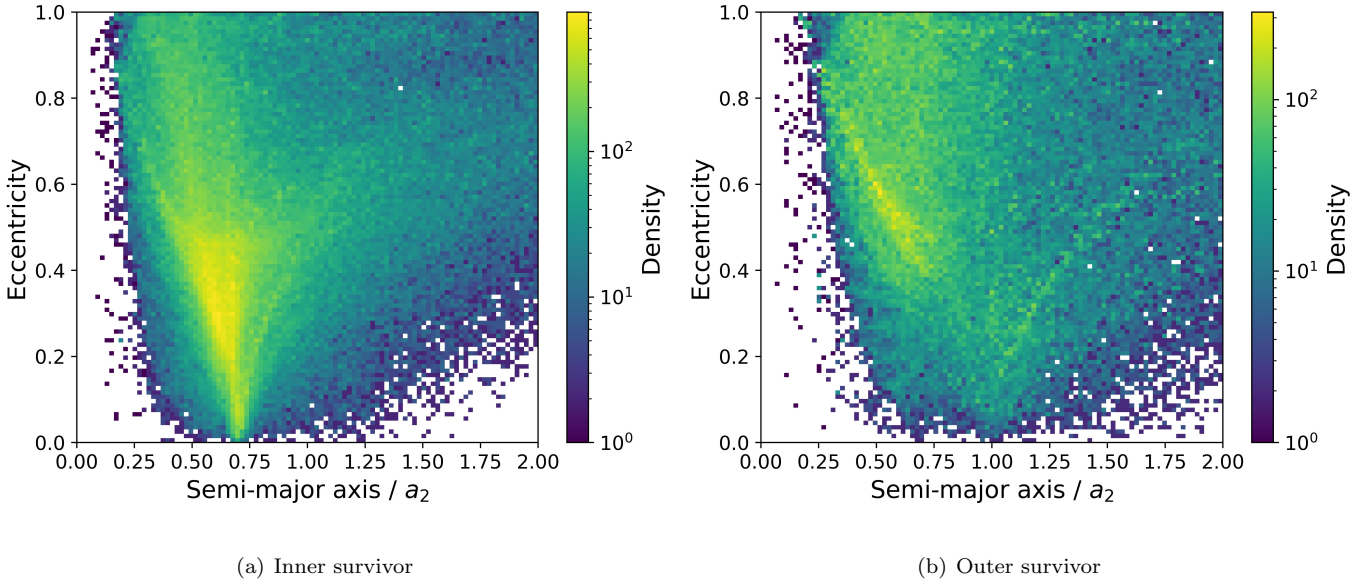


Figure 5. Single planet $e - a$ distribution

3.4. Property of double bound planet

In addition to the formation of the free-floating planet and single planet system, a large part of the situation is that the two planets are still bound by the original stellar gravity after the perturbation. We can analyze the changes in the orbital parameters of these systems in Figure 6.

However, it's important to highlight that the segment of the previous analysis where $q > 2.0$ doesn't require consideration because the likelihood of such scenarios occurring after $q > 2.0$ is extremely low. Nevertheless, the exclusion of $q > 2.0$ truncation in the analyzed case of this section might not be applicable. This is because the flyby still imparts non-negligible disturbances to the system at $q > 2.0$, as evident from B. Additionally, given the relatively short simulation time, uncertainties exist regarding whether the dual planet system will maintain these orbital parameters stably.

3.5. Property of stolen planet

Another phenomenon that can occur in our system is that a planet is gravitationally captured by the flyby, moving from the original star system to a new star system, hence this phenomenon we call planetary exchange. We are curious about what the orbital parameters of the planets exchanged in the star system are, and whether they are clearly different from the orbital parameters of the original planets.

We plot the semi-major axis and eccentricity distribution of the original inner planet and the original outer planet in the new star system in Figure 7. As can be seen from the semi-major axis, the inner planet and the outer planet still have different orbital semi-major axis distributions after the planet exchange. The size of the semi-major axis corresponds to the magnitude of the total orbital energy, so we can also confirm by rescaling a_i whether this is due to a difference in the initial orbital energy. the distribution of the inner and outer planets is very similar after rescaling. with the obvious feature that most of the exchanged planet has a higher eccentricity. The mechanism of this should be different from the one discussed earlier in 3.3.

We can also acquire the e-a plot as well for both inner planet exchange and outer planet exchange in Figure 8. We can still see noticeable envelopes, but there are no very special areas to keep an eye on.

3.6. Property of JuMBO

Recent observations of Jupiter Mass Binary Objects (JuMBOs) can also form in our system, although the probability is very small (less than 0.05% in most q). We can analyze the orbital parameters of these unique systems based on our data. In the pre-study, we found that the probability of JuMBO formation is very sensitive to the spacing between the orbits of the two planets $a_2 - a_1$, and we analyzed the orbital parameters in 2.1 and pointed out that $\frac{a_2}{a_1} = 0.7$ is a relatively stable parameter. In fact, although $\frac{a_2}{a_1} = 0.8$ will cause the star system to be unstable in the long run, in

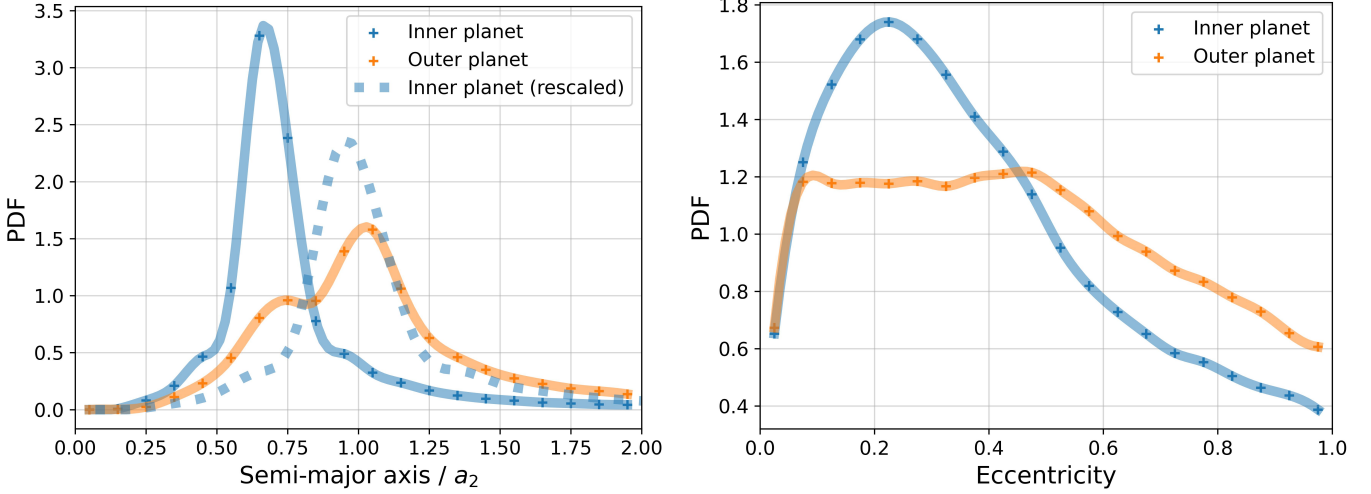


Figure 6. Double bound planet system orbital parameter distribution. In the distribution of the semi-major axis (left panel), the blue dashed line represents the semi-major axis of the inner planet after rescaling. It is evident that the distribution of the semi-major axis in the binary planet system aligns more closely with our expectations, displaying diffusion near the initial value. Nevertheless, the semi-major axis distribution of the outer planet exhibits a plateau around 0.75. This observation corresponds to the inward migration of the semi-major axis distribution, as identified in the intense perturbation analysis of the single planet system discussed earlier. The inner planet experiences minimal migration due to the prevailing influence of data from weak perturbations. As for the eccentricity distribution, it is in line with the analysis in the single planet system analysis. Specifically, smaller perturbations are associated with a lower peak position and greater dispersion in the distribution.

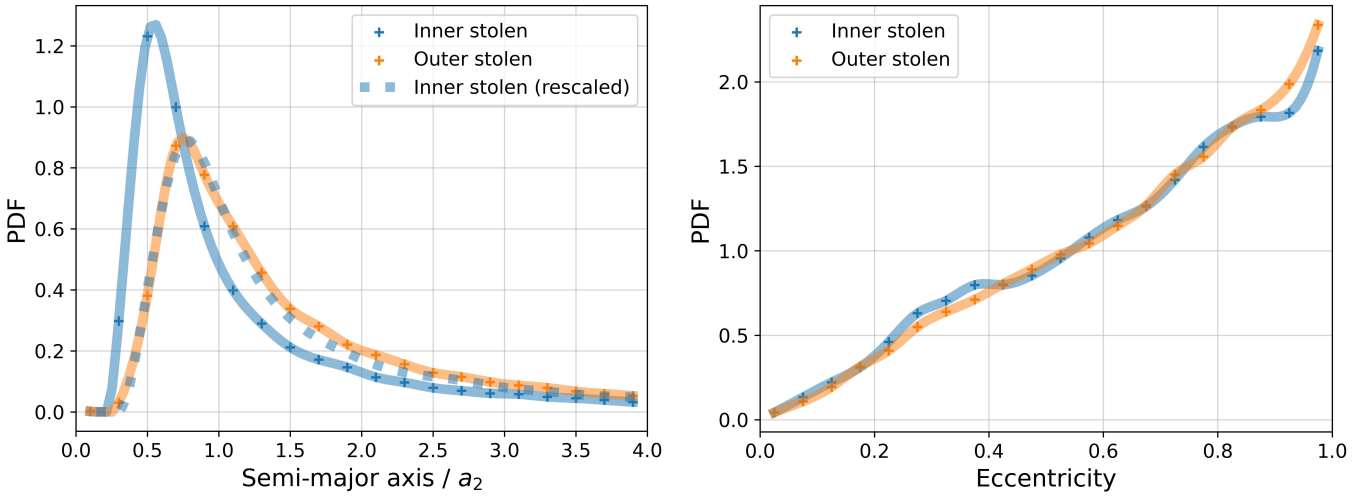


Figure 7. Stolen planet orbital parameter distribution

our simulation, the star system will not be strongly disturbed by the gravitational force between the planets due to the relatively short time from the start of the simulation to the arrival of the flyby to the original star. However, it is worth noting that the probability of generating JuMBOs at $\frac{a_2}{a_1} = 0.8$ is about 17 times that of $\frac{a_2}{a_1} = 0.7$, so we also introduce the JuMBOs orbital parameters generated at $\frac{a_2}{a_1} = 0.8$ for analysis. Here we still sampled $20 \times 20 \times 20 \times 20$ angles (for i , ω , λ_{p1} , and λ_{p2}) for the simulation of $\frac{a_2}{a_1} = 0.8$. However, as we mentioned in 3.1, there are too few valid JuMBO cases under at $\frac{a_2}{a_1} = 0.7$, resulting in a large fluctuation of the data, so we sampled $30 \times 30 \times 30 \times 30$ angles (for i , ω , λ_{p1} , and λ_{p2}) to get more examples.

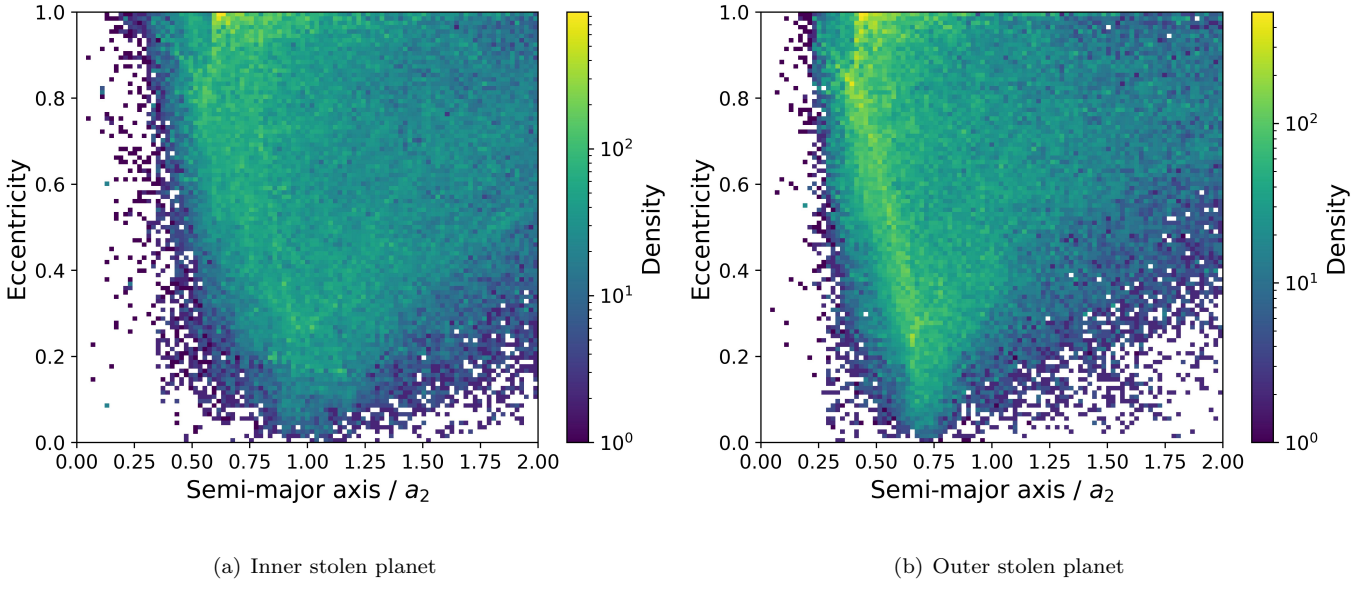


Figure 8. Stolen planet $e - a$ distribution

Finally, we can obtain the distribution of the orbital semi-major axis and eccentricity of JuMBOs corresponding to different $\frac{a_2}{a_1}$ in Figure 9.

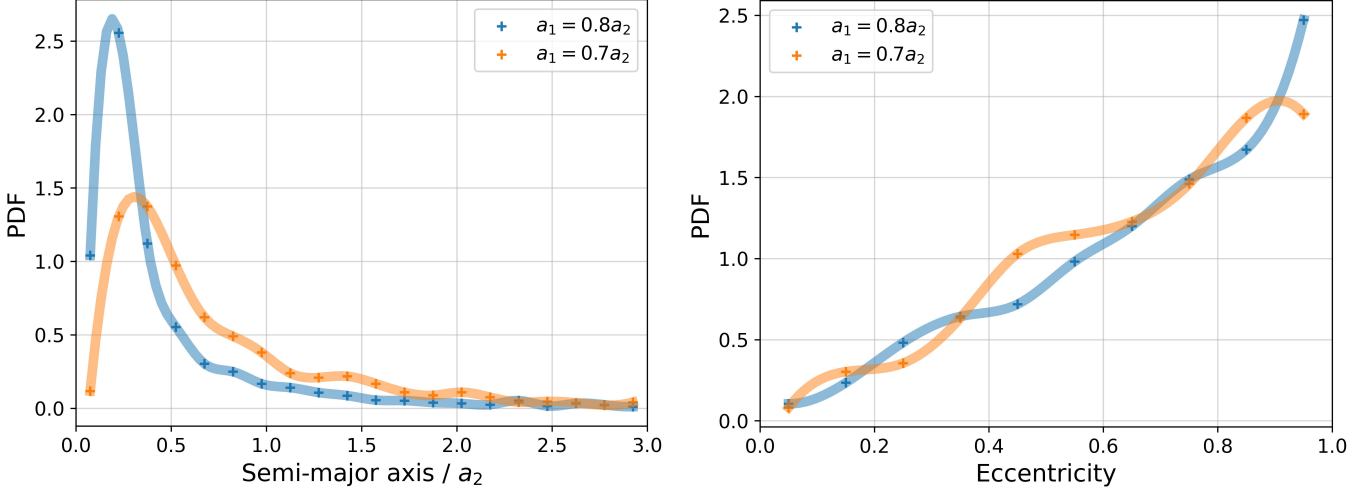


Figure 9. JuMBOs' orbital parameter

It can be seen that the probability decreases rapidly with the increase of the semi-major axis, and the semi-major axis of JuMBO increases as the original interval increases. At the same time, the peak of the semi-major axis distribution roughly match the interval between the planetary orbits at the initial time $a_2 - a_1$. JuMBO is also more likely to have a greater eccentricity. This suggests that the orbit of JuMBO is more elliptical.

We can also acquire the e-a plot of JuMBOs when $\frac{a_2}{a_1} = 0.8$ in Figure 10. The conclusion that JuMBO's orbit is more elliptical is even more pronounced in this figure.

4. OCCURENCE RATE

In stellar cluster, we know that Stellar Density Distribution $dn_*(v_\infty)$, which is a function of the velocity distribution f of the stellar velocities v_∞ . We take f to be a Maxwell–Boltzmann distribution with dispersion σ_* :

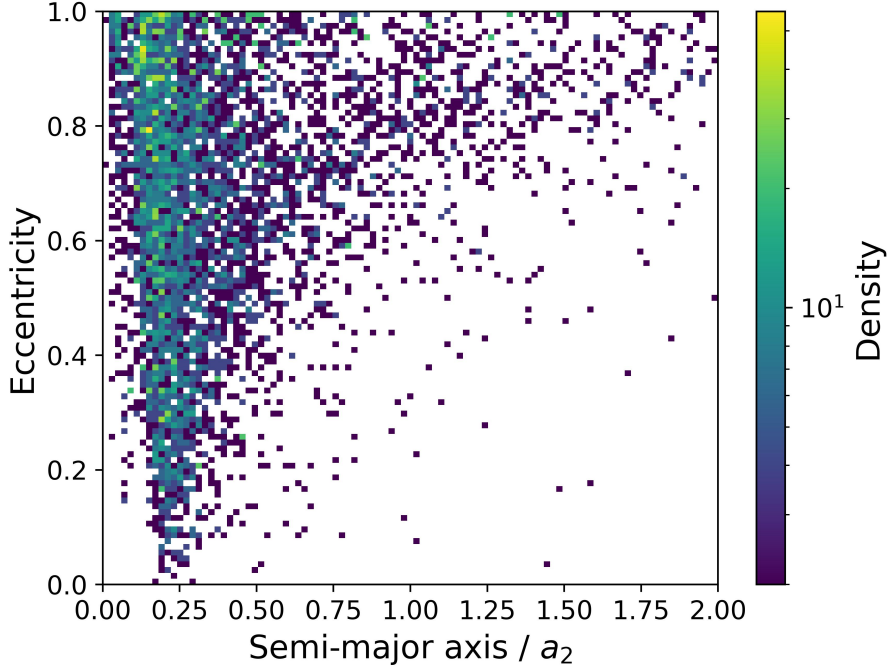


Figure 10. JuMBOs' e-a distribution

$$dn_{\star} = n_{\star} f(v_{\infty}) dv_{\infty} \quad (4)$$

$$f(v_{\infty}) = \sqrt{\frac{2}{\pi}} \frac{v_{\infty}^2}{\sigma_{\star}^3} \exp\left(-\frac{v_{\infty}^2}{2\sigma_{\star}^2}\right). \quad (5)$$

$$\mathcal{R}_i = \int_0^{\infty} dn_{\star}(v_{\infty}) v_{\infty} \int_0^{+\infty} \pi db^2(q, v_{\infty}) p_i(\tilde{q}); \quad (6)$$

The impact parameter $b(q, v_{\infty})$ associated with an hyperbolic trajectory of periastron q and velocity at infinity v_{∞} is

$$b^2 = q^2 \left(1 + \frac{2GM_{\text{tot}}}{qv_{\infty}^2}\right) \approx \frac{2GM_{\text{tot}}q}{v_{\infty}^2} \quad (7)$$

In our setup, equation (6) then becomes

$$\mathcal{R}_i = \mathcal{R}_{\text{close}} \int_0^{+\infty} d\tilde{q} p_i(\tilde{q}) = \mathcal{R}_{\text{close}} \sum_n p_i(\tilde{q}_n) \Delta \tilde{q}_n \quad (8)$$

where

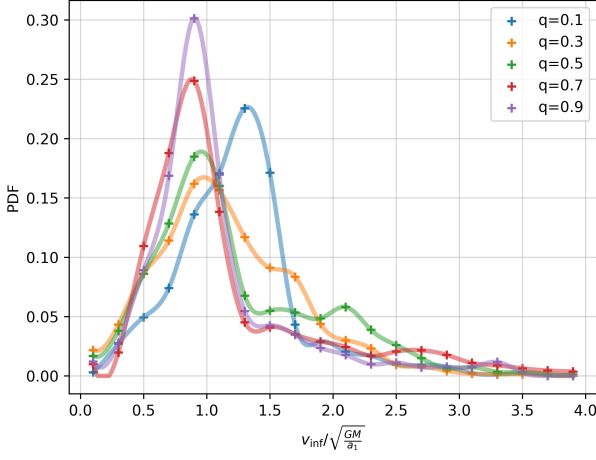
$$\begin{aligned} \mathcal{R}_{\text{close}} &= 2\pi a_p GM_{\text{tot}} n_{\star} \int_0^{\infty} \frac{dv_{\infty}}{v_{\infty}} f(v_{\infty}) \\ &= \frac{2\sqrt{2\pi} a_p GM_{\text{tot}} n_{\star}}{\sigma_{\star}} \\ &\approx 2 \left(\frac{n_{\star}}{10^3 \text{pc}^{-3}}\right) \left(\frac{M_{\text{tot}}}{2M_{\odot}}\right) \left(\frac{a_p}{50 \text{au}}\right) \left(\frac{\sigma_{\star}}{1 \text{kms}^{-1}}\right)^{-1} \text{Gyr}^{-1} \end{aligned} \quad (9)$$

197 For some of the more detailed analyses, and the results corresponding to different disturbance intensities ($\tilde{q} = \frac{a_p}{a_i}$),
 198 we present them in detail in the appendix. For q , we take $q = 1(a_p = a_i)$ as the boundary, and make the orbit
 199 parameters corresponding to 5 different q values in $q < 1$ and 5 orbit parameters corresponding to different q values
 200 in $q > 1$. From these figures we can see the effect of different perturbations on the orbit.

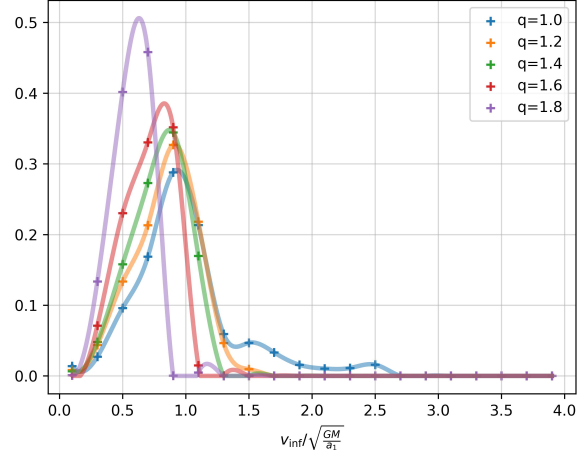
201 In the analysis of the main text, we know that there is no significant difference in the behavior of the inner planet
 202 and the outer planet for most of the phenomena, so we generally only focus on the inner planet when we analyze it in
 203 detail, and we believe that the same applies to the outer planet.

A. FREE-FLOATING PLANETS

205 For free-floating planets, we only care about their v_{inf} . The v_{inf} after different perturbations is shown in Figure 11
 206 and Figure 12.



207 **Figure 11.** Free floating v_{inf} distribution ($q < 1$)



208 **Figure 12.** Free floating v_{inf} distribution ($q > 1$)

209 We can roughly see that when the disturbance is large (q is small), the dispersion of velocity is also larger, but the
 210 position of the peak is basically unchanged.

B. PLANETS REMAIN BOUND

211 Planets remain bound can be divided into three main categories.

- 212 1. In a two-planet system, one planet is kicked out of the system and becomes a free floating planet, and the other
 213 one survives.
- 214 2. In a two-planet system, one planet is flyby captured and the other one survives.
- 215 3. Both planets survived.

216 We analyze the survival of the outer planet in the first two cases. Finally, considering all the planets that are still
 217 gravitationally bound by the original star, we analyze both the inner and outer planets separately, so that the effect
 218 of the perturbation intensity (represented by q) on the orbital parameters can be seen more clearly.

B.1. Survivors after ejection

219 For survivors after ejection, we can plot the orbital semi-major axis and eccentricity for different q respectively in
 220 Figure 13, Figure 14, Figure 15 and Figure 16.

221 We can also see that the distribution of the semi-major axis becomes larger as the perturbation increases, but the
 222 peak value of the distribution is not clearly distinguished, and is still around $0.7a_1$, that is, the initial semi-major axis
 223 of the inner planet.

224 From the distribution of eccentricity, it can be seen that as the perturbation weakens (q becomes larger), the peak
 225 of eccentricity gradually shifts to the left, and the diffusion gradually decreases.

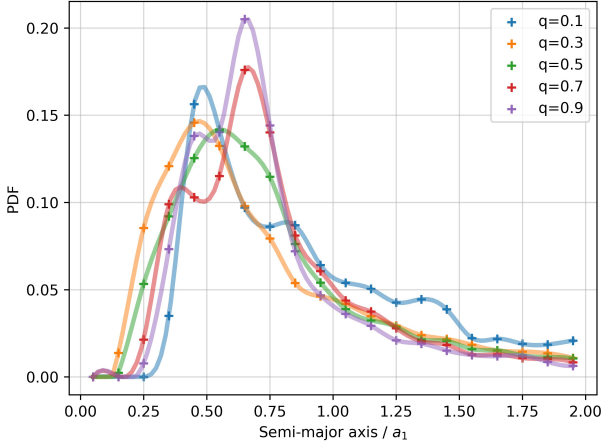


Figure 13. Survivors after ejection semi-major axis distribution ($q < 1$)

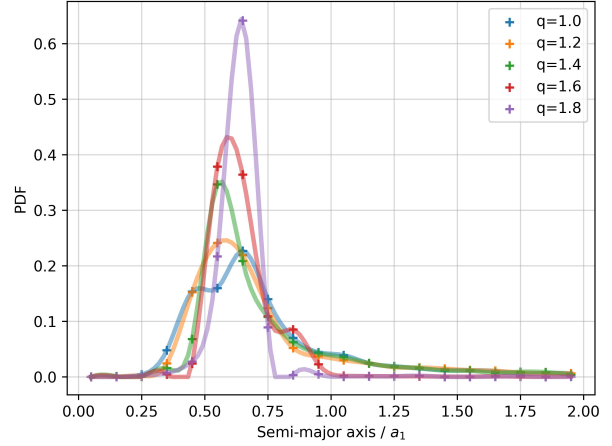


Figure 14. Survivors after ejection semi-major axis distribution ($q > 1$)

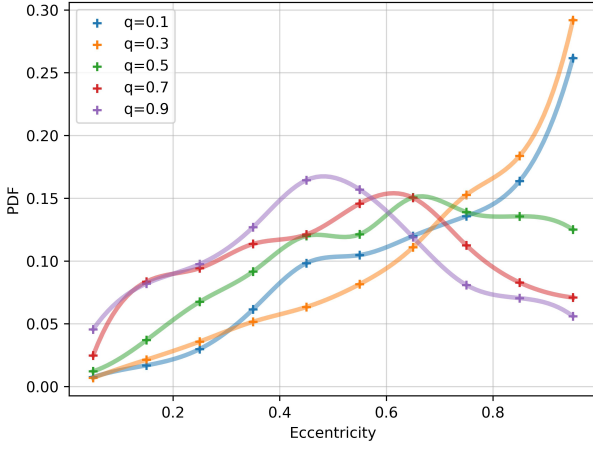


Figure 15. Survivors after ejection eccentricity distribution ($q < 1$)

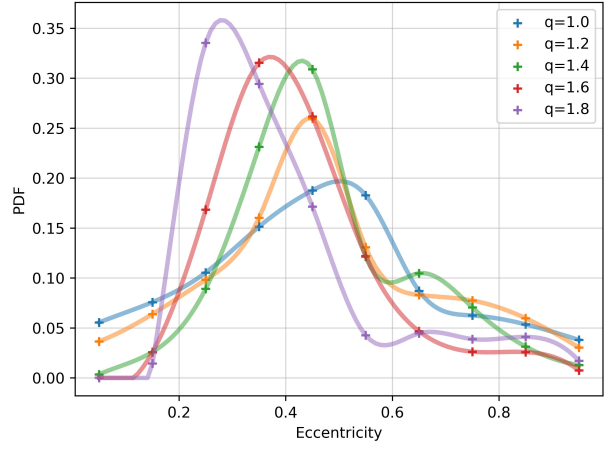


Figure 16. Survivors after ejection eccentricity distribution ($q > 1$)

B.2. Survivors after planet exchange

For survivors after planet exchange, the analysis is roughly the same, and we can get Figure 13, Figure 14, Figure 15 and Figure 16.

As we can see, the situation is almost the same as the previous one. The double-peak-like phenomenon in Figure 20 is actually due to the fact that there is no special mechanism when the perturbation is small (q is large) and the number of cases is smaller, and the fluctuation of the data is larger.

B.3. All bound planets

Finally, we can analyze all planets (including inner planet and outer planet) that are still gravitationally bound by the original star, and get Figure 21 to Figure 28.

It can be seen that the dispersion of the inner bound planet is indeed smaller than that of the outer bound planet, which is in line with our expectations, because the inner planet is less perturbed.

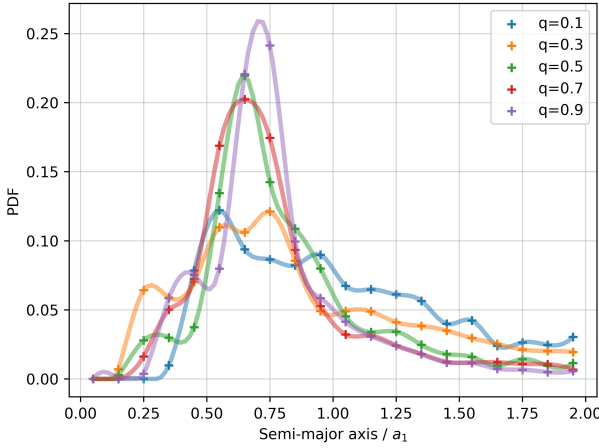


Figure 17. Survivors after planet exchange semi-major axis distribution ($q < 1$)

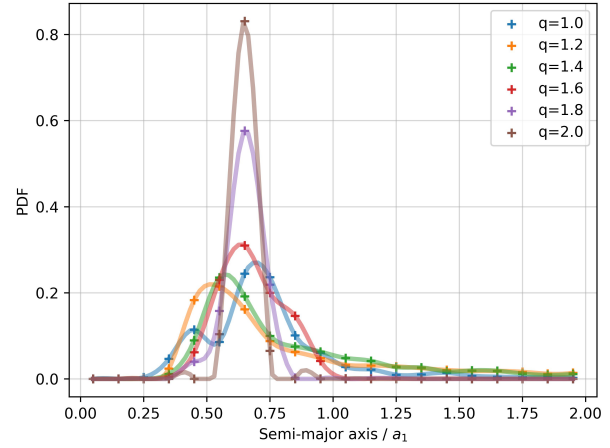


Figure 18. Survivors after planet exchange semi-major axis distribution ($q > 1$)

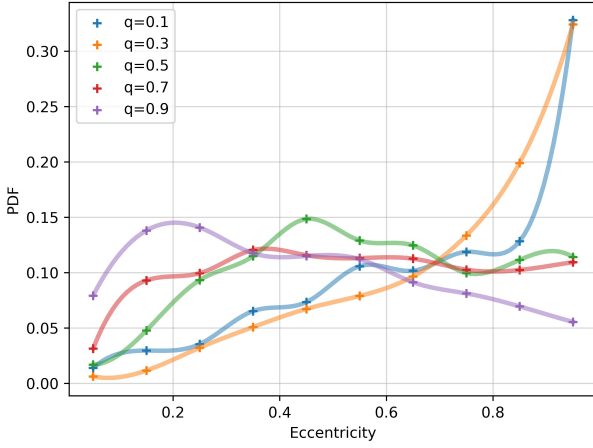


Figure 19. Survivors after planet exchange eccentricity distribution ($q < 1$)

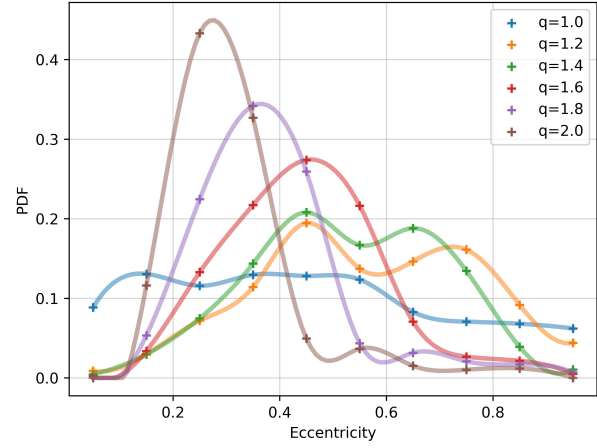


Figure 20. Survivors after planet exchange eccentricity distribution ($q > 1$)

C. EXCHANGED PLANETS

In ?? we analyzed the orbital parameters of the exchanged planets, and now we analyze the orbital parameters of different perturbations in detail to obtain Figure 29 to Figure 32

It can be seen from the Figures that there is no direct relationship between the distribution of eccentricity and the intensity of the disturbance, but the dispersion of the semi-major axis seems to change from small to large and then smaller with q from 2.0 to 0.1, and the dispersion is the largest at $q = 1.0$.

REFERENCES

- 248 Pearson, S. G., & McCaughean, M. J. 2023, Jupiter Mass
249 Binary Objects in the Trapezium Cluster.
250 <https://arxiv.org/abs/2310.01231>
- 251 Rein, H., & Liu, S. F. 2012, A&A, 537, A128,
252 doi: [10.1051/0004-6361/201118085](https://doi.org/10.1051/0004-6361/201118085)
- 253 Rein, H., & Spiegel, D. S. 2015, MNRAS, 446, 1424,
254 doi: [10.1093/mnras/stu2164](https://doi.org/10.1093/mnras/stu2164)
- 255 Rodet, L., Su, Y., & Lai, D. 2021, The Astrophysical
256 Journal, 913, 104, doi: [10.3847/1538-4357/abf8a7](https://doi.org/10.3847/1538-4357/abf8a7)

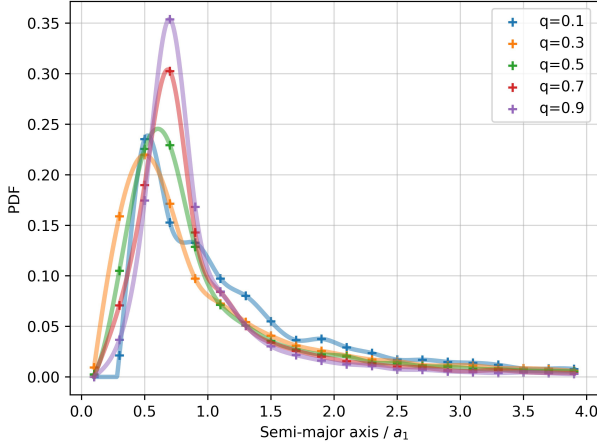


Figure 21. Inner bound planet semi-major axis distribution ($q < 1$)

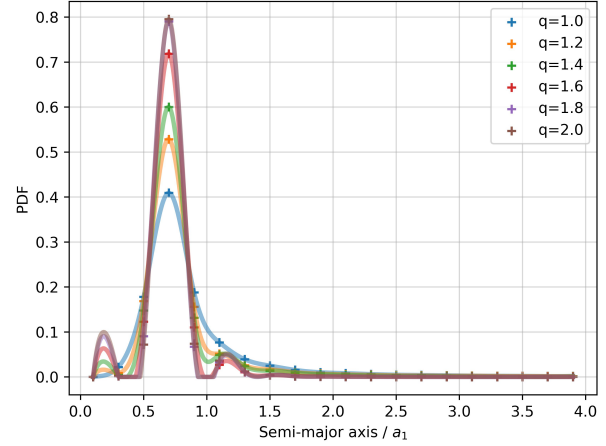


Figure 22. Inner bound planet semi-major axis distribution ($q > 1$)

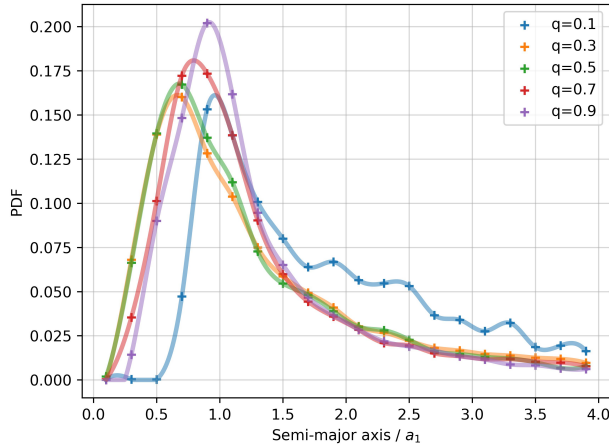


Figure 23. Outer bound planet semi-major axis distribution ($q < 1$)

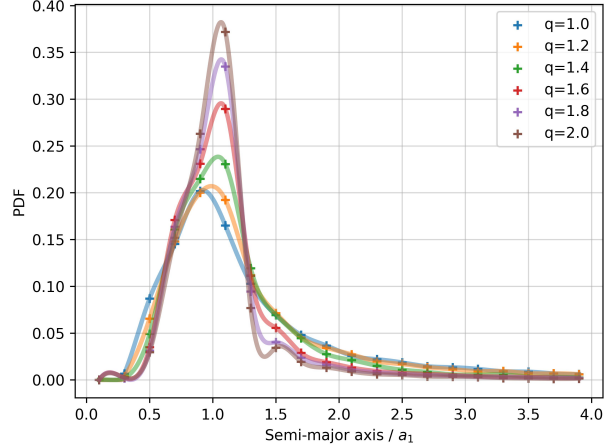


Figure 24. Outer bound planet semi-major axis distribution ($q > 1$)

257 Wang, Y., Perna, R., & Zhu, Z. 2024, Floating binary
 258 planets from ejections during close stellar encounters.
 259 <https://arxiv.org/abs/2310.06016>

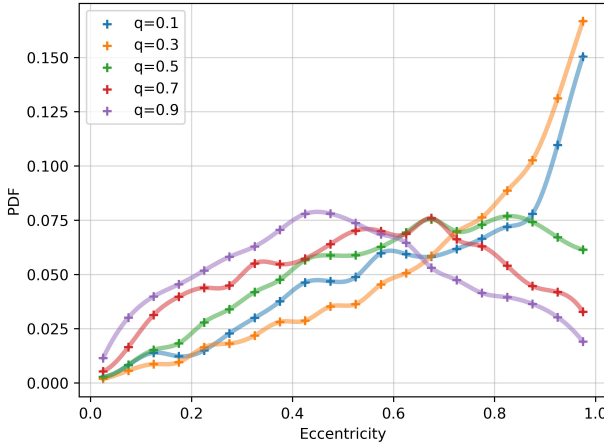


Figure 25. Inner bound planet eccentricity distribution ($q < 1$)

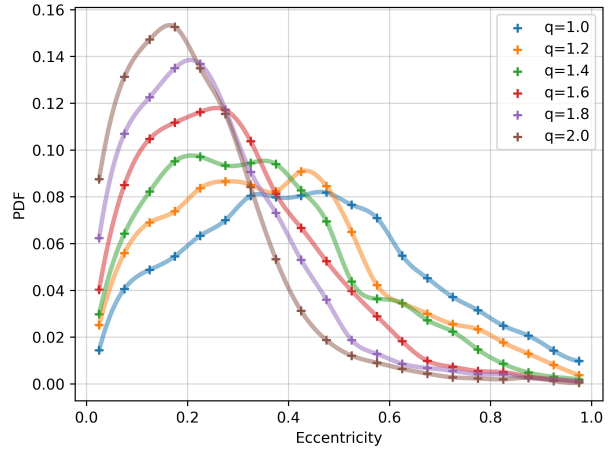


Figure 26. Inner bound planet eccentricity distribution ($q > 1$)

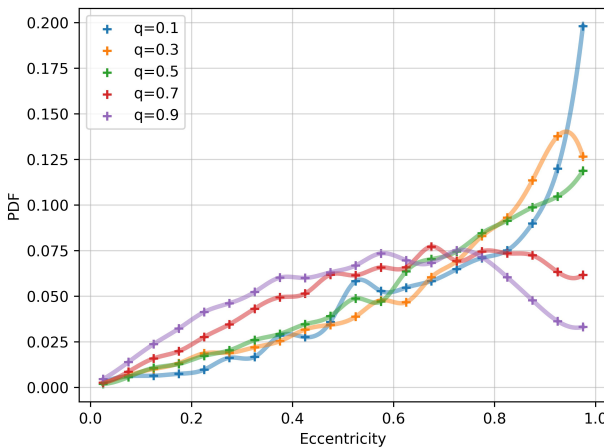


Figure 27. Outer bound planet eccentricity distribution ($q < 1$)

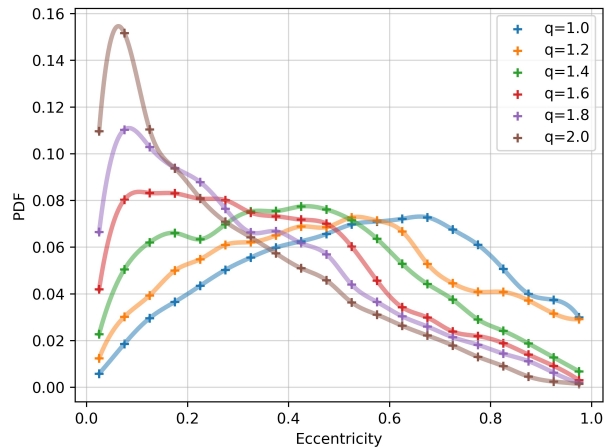


Figure 28. Outer bound planet eccentricity distribution ($q > 1$)

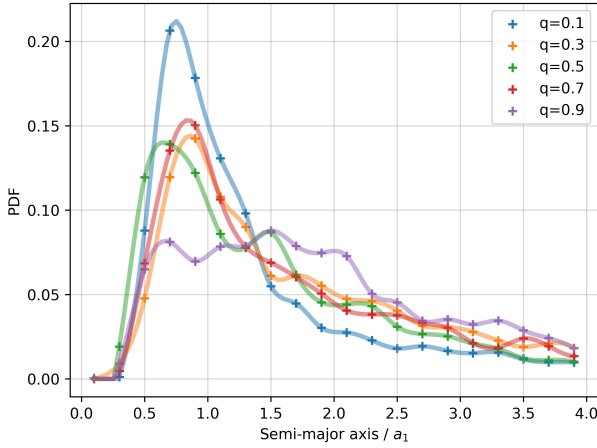


Figure 29. Exchanged planet semi-major axis distribution ($q < 1$)

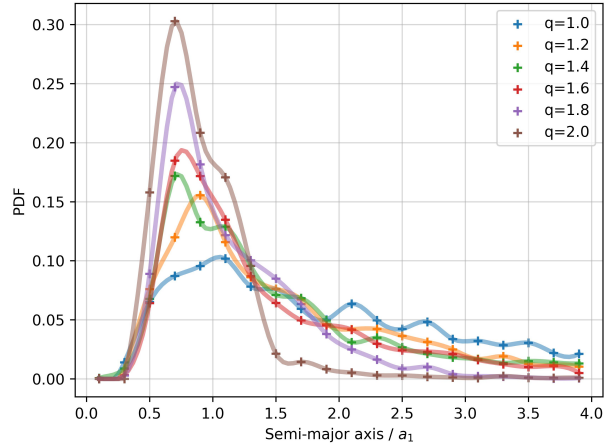


Figure 30. Exchanged planet semi-major axis distribution ($q > 1$)

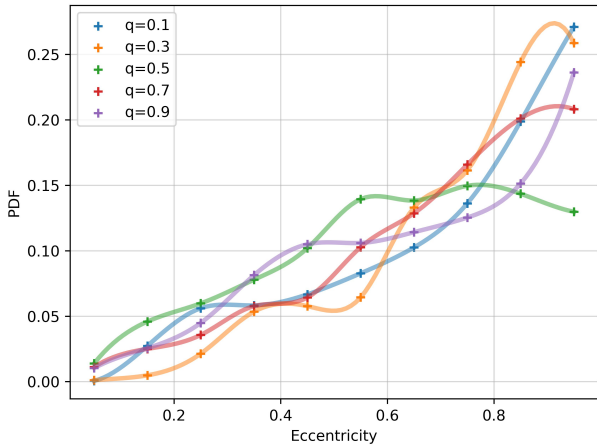


Figure 31. Exchanged planet eccentricity distribution ($q < 1$)

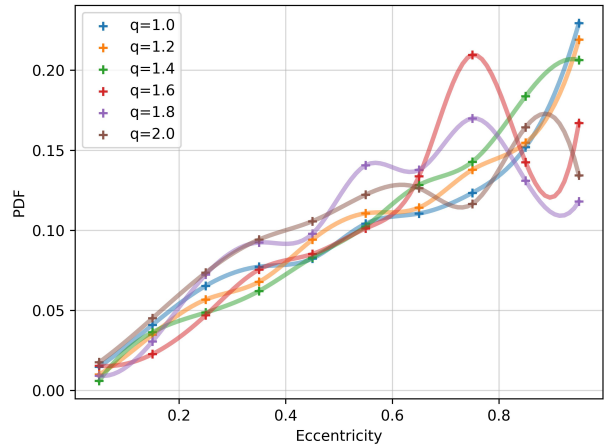


Figure 32. Exchanged planet eccentricity distribution ($q > 1$)